Stress Intensity Factors of Semi-Circular Bend Specimens with Straight-Through and Chevron Notches

M. R. Ayatollahi, E. Mahdavi, M. J. Alborzi & Y. Obara

Rock Mechanics and Rock Engineering

ISSN 0723-2632
Volume 49
Number 4

Rock Mech Rock Eng (2016)
49:1161-1172
DOI 10.1007/s00603-015-0830-y

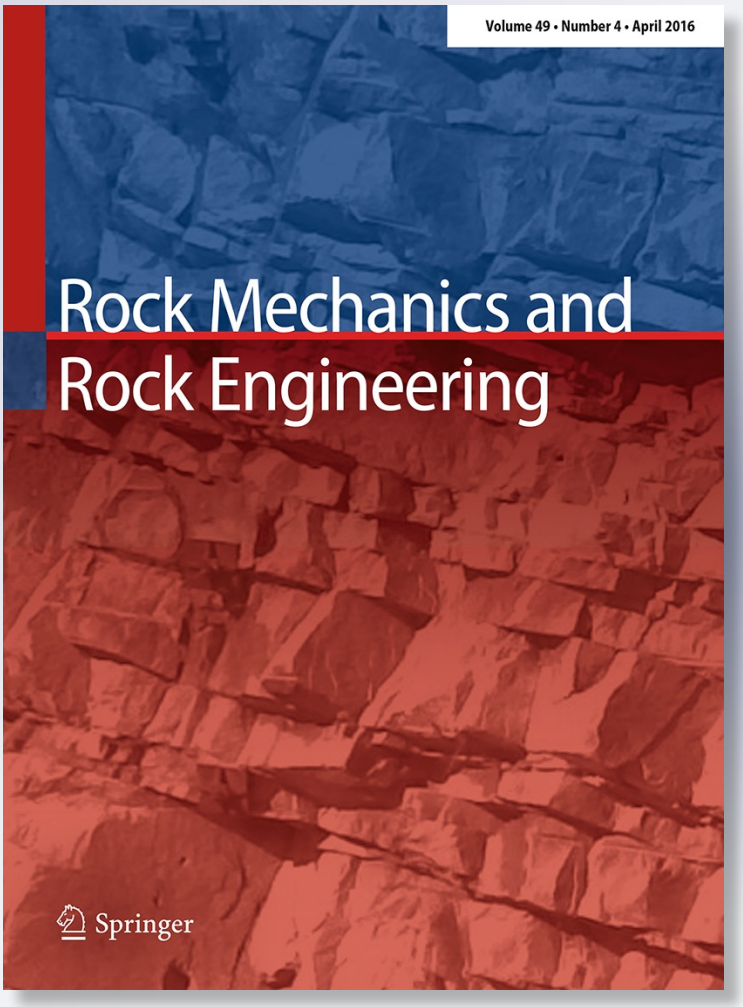

Springer

Rock Mech Rock Eng (2016) 49:1161–1172
DOI 10.1007/s00603-015-0830-y

ORIGINAL PAPER

Stress Intensity Factors of Semi-Circular Bend Specimens with Straight-Through and Chevron Notches

M. R. Ayatollahi[1] · E. Mahdavi[1] · M. J. Alborzi[1] · Y. Obara[2]

Received: 5 January 2015 / Accepted: 23 August 2015 / Published online: 2 September 2015

Abstract Semi-circular bend specimen is one of the useful test specimens for determining fracture toughness of rock and geo-materials. Generally, in rock test specimens, initial cracks are produced in two shapes: straight-edge cracks and chevron notches. In this study, the minimum dimensionless stress intensity factors of semi-circular bend specimen (SCB) with straight-through and chevron notches are calculated. First, using finite element analysis, a suitable relation for the dimensionless stress intensity factor of SCB with straight-through crack is presented based on the normalized crack length and half-distance between supports. For evaluating the validity and accuracy of this relation, the obtained results are then compared with numerical and experimental results reported in the literature. Subsequently, by performing some experiments and also finite element analysis of the SCB specimen with chevron notch, the minimum dimensionless stress intensity factor of this specimen is obtained. Using the new equation for the dimensionless stress intensity factor of SCB with straight-through crack and an analytical method, i.e., Bluhm's slice synthesis method, the minimum (critical) dimensionless stress intensity factor of chevron notched semi-circular bend specimens is calculated. Good agreement is observed between the results of two mentioned methods.

✉ M. R. Ayatollahi
m.ayat@iust.ac.ir

[1] Fatigue and Fracture Laboratory, Center of Excellence in Experimental Solid Mechanic and Dynamics, School of Mechanical Engineering, Iran University of Science and Technology, Narmak, 16846 Tehran, Iran

[2] Graduate School of Science and Technology, Kumamoto University, Kumamoto, Japan

Keywords Rock fracture mechanics · Semi-circular bend specimen · Chevron notch · Stress intensity factor · Finite element modeling

Abbreviations

a	Crack length
a_m	Critical crack length
a_0	Initial crack length
a_1	Final crack length
b	Crack front width
B	Thickness of specimen
E	Young's modulus
h_c	Cutting depth of chevron notch
i	Slice number in slice synthesis method
K_I	Mode-I stress intensity factor
K_{Ic}	Mode-I fracture toughness
n	Constant in reduction factor formulation of slice synthesis method
N	Number of slices in slice synthesis method
P	Load
P_{max}	Measured maximum load
R	Radius of specimen
Rs	Radius of rotary saw
S	Half-distance between the supports
Y_I	Mode-I dimensionless stress intensity factor
Y^*	Dimensionless stress intensity factor of specimen
Y^*_{min}	Minimum dimensionless stress intensity factor of specimen
α	Normalized crack length
α_B	Normalized thickness
α_m	Normalized critical crack length
α_s	Normalized radius of rotary saw
α_0	Normalized initial crack length
α_1	Normalized final crack length

β	Reduction factor in slice synthesis method
Δt	Thickness of slice in slice synthesis method
ε_x	Strain component in x direction
ε_y	Strain component in y direction
ε_z	Strain component in z direction
γ	Geometry factor in slice synthesis method
v	Poisson's ratio
CB	Chevron bend specimen
CCNBD	Cracked chevron notched Brazilian disc
CCNSCB	Cracked chevron notched semi-circular bend specimen
CSTSCB	Cracked straight through semi-circular bend specimen
FEM	Finite element method
ISRM	International society for rock mechanics
LEFM	Linear elastic fracture mechanics
SCB	Semi-circular bend specimen
SIF	Stress intensity factor
SR	Short rod specimen
SSM	Slice synthesis method

1 Introduction

Fracture mechanics is employed as a useful tool to solve various rock engineering problems such as rock cutting, hydraulic fracturing, blasting, stability of rocks, etc. The linear elastic fracture mechanics (LEFM) is mainly an extension of Griffith's theory and Irwin's modification that identifies the importance of stress intensity factor. Irwin used stress intensity factor (SIF) as a parameter to describe the stress and the displacement fields near a crack tip.

Fracture toughness is considered as a main parameter in fracture mechanics that describes the material resistance to propagation of pre-existing cracks (Kanninen and Popelar 1985). Indeed, fracture toughness can also be explained as a critical value of SIF when a crack propagates. Therefore, if the SIF is known for a given body under a definite type and magnitude of loading, the fracture toughness can be determined from a fracture test.

Four testing methods have been suggested by the International Society for Rock Mechanics (ISRM) for measuring rock fracture toughness: (a) short rod specimen method (SR) (Matsuki et al. 1991; Ouchterlony 1998); (b) chevron bend specimen method (CB) (Ouchterlony 1998); (c) cracked chevron notched Brazilian disc (CCNBD) specimen method (Fowell 1995) and cracked straight through semi-circular bend specimen (CSTSCB) (Kuruppu et al. 2014).

The semi-circular bend (SCB) specimen proposed initially by Chong et al. (1987) has recently received much attention by researchers (Lim et al. 1993, 1994; Kuruppu 1997, 1998, 2000; Kuruppu and Chong 2012; Kuruppu et al. 2014). Some advantages of the SCB specimens are convenient sample preparation (directly from rock cores), simple geometry and loading configuration, the straightforward testing procedure and application of compressive load, which is more suitable for rocks, rather than tensile load. Furthermore, SCB is a suitable specimen to measure the rock fracture toughness at elevated temperatures, high strain rates, and high confining pressures (Kuruppu and Chong 2012).

Crack in rock test specimens can be created with either a straight or a chevron shape, as shown in Fig. 1b, c, respectively. In general, according to ISRM suggested methods for determining fracture toughness of rocks, the chevron notch has some advantages over a straight one. There is a very high stress concentration at the chevron notch tip. Therefore, the crack initiates at a very low load level from the chevron notch tip and grows to a specific distance in a stable manner, and then sudden failure takes place. As a result, the fatigue pre-cracking is unnecessary in this specimen, whereas in the straight-through crack specimen, either fatigue pre-cracking is needed that is very difficult for brittle and quasi-brittle materials or the crack

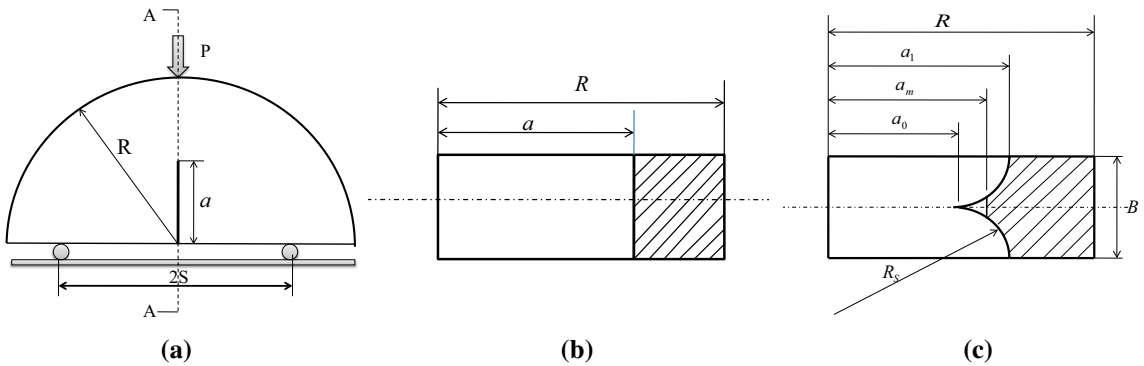

Fig. 1 **a** Semi-circular bend specimen geometry and loading configuration, **b** straight-through crack, and **c** chevron notch

must be generated by a very thin saw blade which sometimes is not easy.

So far, the cracked chevron notched semi-circular bend (CCNSCB) specimen has been less considered in SCB testing. Only, a limited calibration of stress intensity factors was performed using a three-dimensional finite element simulation (Kuruppu 1997, 1998, 2000).

Geometrical parameters in a CCNSCB specimen of radius R can be found in Fig. 1c in which $\alpha_0 = (a_0/R)$, $\alpha_1 = (a_1/R)$, and $\alpha_m = (a_m/R)$ are the normalized initial, final, and critical crack lengths, respectively, α_s is the normalized radius of rotary saw (R_s/R) and $\alpha_B = B/R$ is the normalized thickness.

The aim of this study is to calculate the dimensionless stress intensity factors of CCNSCB and CSTSCB specimens. Using finite element analysis, suitable relations for dimensionless stress intensity factor of CSTSCB specimen are presented. By comparing the results obtained from these equations with limited numerical results reported in the previous papers, their validity is investigated. For CCNSCB, at first, some experimental tests are conducted to find the maximum load of this specimen. Then, CCNSCB is analyzed using the maximum experimental load and finite element analysis to obtain the critical dimensionless stress intensity factor and critical crack length. Thereafter, using the new relation of dimensionless stress intensity factor for CSTSCB specimen and an analytical method, i.e., Bluhm's slice synthesis method, the minimum dimensionless stress intensity factor of CCNSCB specimens are determined analytically.

2 Evaluation of Stress Intensity Factor for Semi-Circular Bend Specimens

2.1 Cracked Straight Through Semi-Circular Bend Specimen (CSTSCB)

Fracture toughness of CSTSCB specimen in mode-I can be determined as (Kuruppu et al. 2014)

$$K_{Ic} = \frac{P_{\max}\sqrt{\pi a}}{2RB} Y_I(a/R, S/R), \tag{1}$$

where P_{max} is the measured maximum load, B is the thickness of specimen, Y_I is the mode-I dimensionless stress intensity factor, a and R are the crack length and the radius of the specimen, respectively, and S is the half-distance between the supports. As an important parameter in determining the material fracture toughness, the geometry factor Y_I is specified as a function of a/R and S/R (Lim et al. 1994). Using the classical displacement extrapolation technique, the SIF of CSTSCB specimen from finite element analysis in terms of a/R and S/R was obtained, as follows (Lim et al. 1993):

$$Y_I = S/R\big(2.91 + 54.39\alpha - 391.4\alpha^2 + 1210.6\alpha^3 - 1650\alpha^4 + 875.9\alpha^5\big), \tag{2}$$

where α is the ratio of the crack length to the sample radius (a/R).

In the following, the finite element analysis of CSTSCB specimens with different values of crack lengths and support distances are employed in order to calculate the values of stress intensity factors and the results are then compared to the previously reported results (including those of Eq. 2).

The finite element model of CSTSCB specimen can be seen in Fig. 2. The mechanical properties were selected as $E = 2940$ MPa and $\nu = 0.3$. The radius, R and the thickness of specimens were taken as 50 and 5 mm, respectively, and the reference applied compression load P was 10 kN.

A total number of 3000 four-node elements were used to mesh a 2D model of specimen. Because of singularity at the crack tip, the singular and smaller eight-node elements were used around the crack tip as shown in Fig. 2.

In these models, the ranges of α and S/R were both selected between 0.2 and 0.8. The J-integral method was used for calculating the stress intensity factor. The values of stress intensity factors obtained from the finite element modeling for different ratios of α and S/R are shown in Table 1.

Now, the dimensionless stress intensity factor Y_I can be derived from Eq. 1. Using the least-square method for curve fitting, Eq. 3 is obtained for calculating the dimensionless stress intensity factor of CSTSCB specimen. Figure 3 shows the curves of dimensionless stress intensity factors for different values of α and S/R based on Eq. 3 together with the relevant finite element data.

$$\begin{aligned} Y_I = {} & (0.4122 + 5.06355(S/R)) + (-16.65 + 3.319(S/R))\alpha \\ & + (52.939 + 76.910(S/R))\alpha^2 \\ & + (-67.027 - 257.726(S/R))\alpha^3 \\ & + (29.247 + 252.8(S/R))\alpha^4 \end{aligned} \tag{3}$$

As can be seen from Eq. 3, Y_I is linear in terms of S/R and is of fourth order in terms of α.

If the normalized crack length (α) is considered only in the range of 0.2 to 0.6 (more practical than $0.2 \le \alpha \le 0.8$), Eq. 4 which is a second order function in terms of α, could be fitted to the results. Figure 4 shows the curves fitted to the FE results using Eq. 4.

$$\begin{aligned} Y_I = {} & -1.297 + 9.516(S/R) + (-0.47 - 16.457(S/R))\alpha \\ & + (1.071 + 34.401(S/R))\alpha^2 \end{aligned} \tag{4}$$

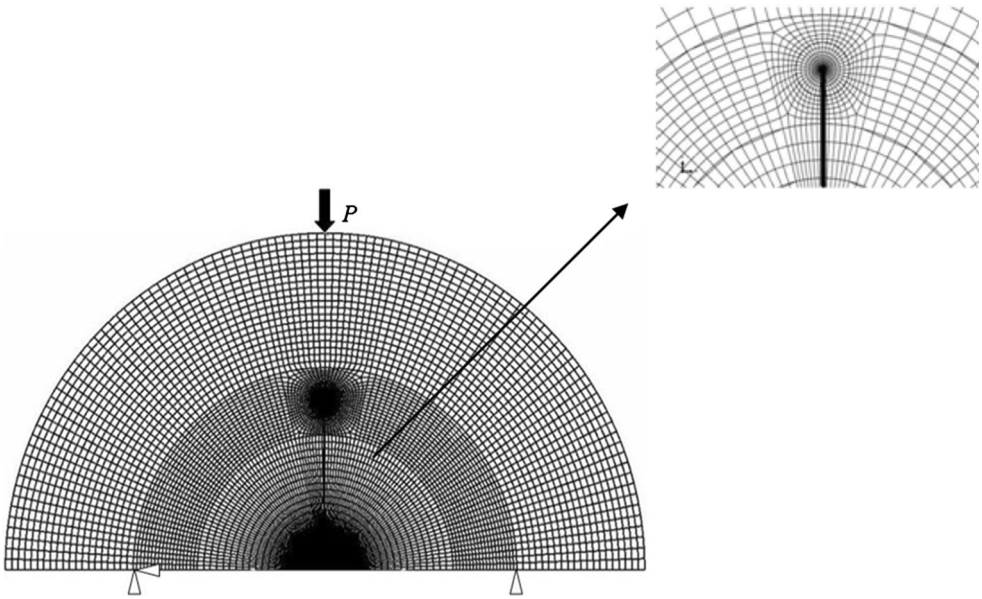

Fig. 2 A typical finite element mesh used for simulating CSTSCB specimen

Table 1 Stress intensity factors for different values of α and *S*/*R* in CSTSCB specimens (in MPa$\sqrt{\text{m}}$)

a/*R*	*S*/*R*						
	0.2	0.3	0.4	0.5	0.6	0.7	0.8
0.2	0.0116	3.542	6.428	8.946	11.358	13.792	16.312
0.3	0.508	4.289	7.859	11.215	14.469	17.713	21.016
0.4	1.876	6.156	10.443	14.685	18.862	23.067	27.391
0.5	3.987	9.365	14.794	20.24	25.706	31.196	36.623
0.6	7.496	14.873	22.315	29.75	37.245	44.715	52.171
0.7	14.272	25.479	36.713	47.979	59.348	70.666	81.801
0.8	30.902	51.181	71.485	91.872	112.1	132.36	152.73

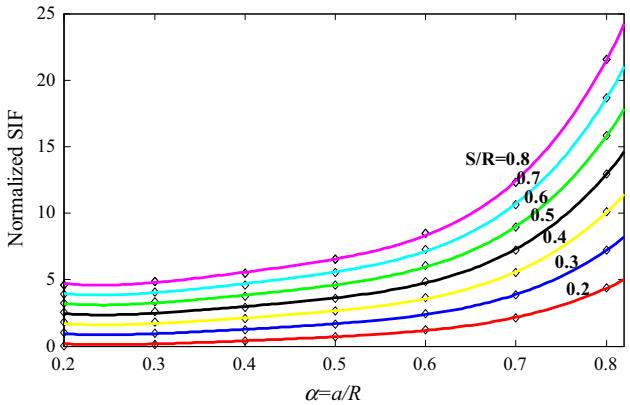

Fig. 3 Dimensionless stress intensity factors for different values of α ($0.2 \le \alpha \le 0.8$) and *S*/*R* ($0.2 \le S/R \le 0.8$) in CSTSCB specimen

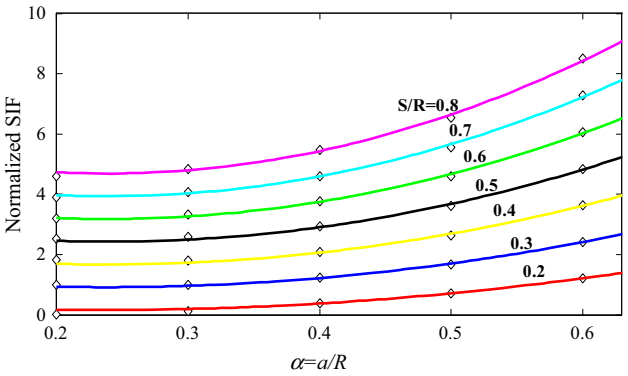

Fig. 4 The values of dimensionless stress intensity factors of CSTCSB specimen for $0.2 \le \alpha \le 0.6$ and $0.2 \le S/R \le 0.8$

Obviously, Eq. 4 is simpler and easier to use than Eq. 3. Furthermore, practically, most of the experiments are carried out with values of α between 0.2 and 0.6.

A comparison between the results obtained from Eqs. 3 and 4 and those of other papers (Lim et al. 1994; Ayatollahi et al. 2006, 2011; Ayatollahi and Aliha 2006; Tutluoglu and Keles 2011) is presented in Table 2. It could be

Table 2 Comparison of mode-I dimensionless stress intensity factors obtained by several researchers

α	S/R	Our results		Other researchers		
		Equation 3	Equation 4	Equation 2 (Lim et al. 1994)	Ayatollahi et al.	Tutluoglu and Keles (2011)
0.2	0.4	1.569	1.692	2.182	–	–
0.2	0.5	2.284	2.452	2.728	–	–
0.2	0.6	2.998	3.212	3.274	–	–
0.3	0.2	0.2231	0.193	1.090	–	–
0.3	0.43	2.079	1.958	2.343	2.057 (Ayatollahi et al. 2006)	–
0.3	0.5	2.644	2.495	2.725	2.604 (Ayatollahi and Aliha 2006)	2.538
0.4	0.2	0.4165	0.373	1.249	–	–
0.4	0.4	2.1513	2.061	2.499	2.152 (Ayatollahi and Aliha 2006)	–
0.5	0.5	3.539	3.679	3.913	3.6 (Ayatollahi et al. 2011)	3.550
0.5	0.6	4.493	4.668	4.696	–	–
0.5	0.3	1.632	1.702	2.725	–	–
0.6	0.3	2.344	2.414	3.119	–	–
0.6	0.8	8.263	8.427	8.319	–	–
0.6	0.69	6.960	7.104	9.025	7.202 (Ayatollahi and Aliha 2006)	–
0.7	0.4	5.678	–	6.192	–	–
0.8	0.5	12.901	–	13.464	–	12.665

observed that Eq. 2 proposed by Lim et al. (1994) for the dimensionless stress intensity factor (fifth column) exhibits higher difference percentages compared to other results. In some cases, e.g., $S/R = 0.69$ and $\alpha = 0.6$, the difference between Eq. 2 and FE results is about 25 %, while in the same case, the difference between the proposed equation, i.e., Eq. 3 and FE value is 3.3 %. In the case of $\alpha = 0.5$ and $S/R = 0.5$, the discrepancy between Eq. 2 and the numerical value given by Tutluoglu and Keles (2011) is 10.2 %, while this discrepancy is about 0.3 % for Eq. 3. Furthermore, it could be found that in smaller ratios of α and S/R (e.g., $\alpha = 0.3$ and $S/R = 0.2$), the differences between the proposed equations (i.e., Eqs. 3 and 4) and Eq. 2 are more than 80 % indicating lower precision of Eq. 2 in small crack lengths.

The lower precision of Eq. 2 could be due to the fact that Lim et al. (1994) has employed the nodal displacement extrapolation method that was a common method in 1990s in order to obtain the stress intensity factor. This method is known to have lower precision compared to the J-integral technique as an alternative method, which has less numerical errors in the region of high stress gradient around the crack tip (Kuruppu et al. 2014). Therefore, Eq. 3 for $0.2 \leq \alpha \leq 0.8$ and $0.2 \leq S/R \leq 0.8$ and Eq. 4 for $0.2 \leq \alpha \leq 0.6$ and $0.2 \leq S/R \leq 0.8$ could be employed as more accurate relations to compute the dimensionless stress intensity factor of CSTSCB specimen.

2.2 Chevron Notched Semi-Circular Bend Specimen (CCNSCB)

Similar to the formulation proposed by ISRM to calculate the rock fracture toughness of CCNBD specimen (Fowell 1995), the following formulation could be written for CCNSCB

$$K_{Ic} = \frac{P_{\max}}{B\sqrt{R}} Y^*_{\min} \tag{5}$$

in which K_{Ic} is the critical stress intensity factor corresponding to the initiation of fracture, $Y^*_{\min}$ is the minimum dimensionless stress intensity factor for mode-I loading, $P_{\max}$ is the experimental peak load, B and R are the thickness and radius of SCB specimen, respectively. It should be noted that, similar to other standard cracked specimens, in order to satisfy the plane strain condition and consistent test results, the geometrical dimensions of SCB specimens should have some limitations. Therefore, for each specimen, the plane strain condition should be studied.

Until now, various methods have been employed in the CCNBD specimens for determining $Y^*_{\min}$; however, applicability and accuracy of none of these methods have been investigated for CCNSCB specimens. In the following, some experimental tests are conducted in order to obtain the experimental maximum load of CCNSCB specimens.

Then, CCNSCB specimen is analyzed by the commercial finite element software ABAQUS. 3D modeling of CCNSCB is used to calculate the distribution of stress intensity factor along the crack front. Thereafter, an analytical method, i.e., slice synthesis method (SSM), which has been previously used to determine the stress intensity factor of CCNBD specimens, will be described. Then, the stress intensity factor of CCNSCB specimen is obtained using this analytical method and is compared with FEM result.

2.2.1 Experiments

In this step, some experiments were conducted to obtain the experimental peak load. The fracture toughness of CCNSCB specimens was then obtained from finite element modeling.

In order to conduct the fracture tests and determine the maximum load of CCNSCB specimen, a type of crystalline rock called Vietnam white marble was selected. The chosen rock contained very few discontinuities; so, it could be considered as an isotropic and homogeneous material.

The rock specimens were prepared using the water jet technique, in the form of semi-circles with 80 mm diameter and 20 mm thickness. A diamond rotary saw of radius 25 mm (R_s) and thickness of 0.6 mm was selected to produce the chevron notch. The advancement of the cutter h_c and the half-distance between the supports S were 11 and 20 mm, respectively. Geometric properties of the specimen are presented in Table 3. A universal tension/compression test machine (SANTAM/STM-150) with a capacity of 15 kN was used to perform the fracture tests. As shown in Fig. 5, three-point bending fixture was employed to apply the load.

The tests were performed on six identical specimens in order to increase the accuracy of results. When the load reached its critical value, sudden failure occurred for all of the specimens and the maximum load was recorded as the critical (fracture) load. The fracture loads obtained from the tests and the corresponding average value are listed in Table 4.

Table 3 Dimensional parameters of tested CCNSCB specimen

Description	Value (mm)	Normalized value
Radius R	40	–
Thickness B	20	$\alpha_B = 0.5$
Initial crack length a_0	7	$\alpha_0 = 0.175$
Final crack length a_1	20.8	$\alpha_1 = 0.52$
Saw radius R_s	25	$\alpha_s = 0.625$
Cutting depth h_c	11	–
Supports distance, $2S$	40	$S/R = 0.5$

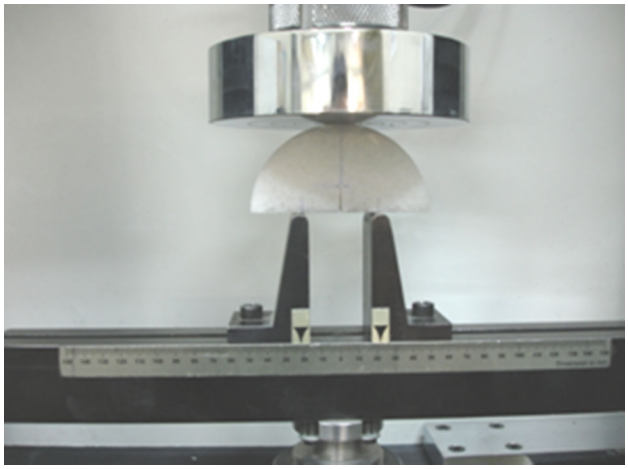

Fig. 5 Loading fixture of SCB specimen

Table 4 The values of fracture loads for CCNSCB specimens

Test no.	P_{max} (kN)
1	1.914
2	1.82
3	1.8
4	1.871
5	1.876
6	1.981
Average	1.877

In the following, the mode-I fracture toughness of CCNSCB specimen was calculated using the average fracture load and employing the finite element analysis in ABAQUS software based on the J-integral method. It is noteworthy that in general, it is not necessary to use only the fracture load to obtain the minimum dimensionless stress intensity factor for a chevron notched specimen; and any other arbitrary reference load can also be used for this purpose. However, because one of the aims in this study was to measure the fracture toughness of the tested material, the average fracture load obtained from the experiments was adapted as reference load.

2.2.2 Finite Element Analysis of CCNSCB Specimen

In finite element modeling, due to symmetry in mode-I loading, only one-half of the specimen was analyzed with appropriate constraints across the symmetry plane. To obtain the mesh convergence in a small-strain analysis, strain singularity near the crack front should be considered. On the other hand, to employ the wedge elements around the crack front and hexahedral elements for remainder of the model, collapsed elements were introduced in a ring partition around the crack front. As a result, fine mesh with singular and collapsed elements were used around the

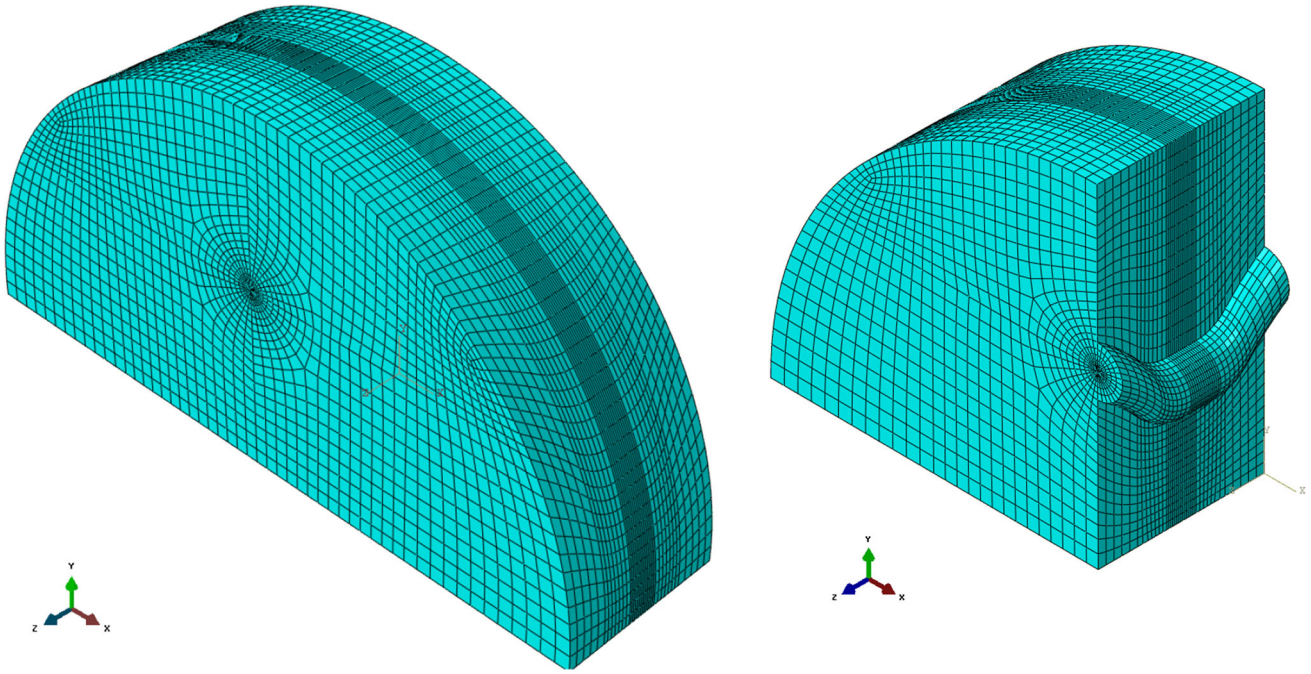

Fig. 6 A typical finite element mesh used for simulating CCNSCB specimen

crack front. Figure 6 shows a typical mesh pattern with approximately 50000 20-node 3D elements developed for simulating the CCNSCB specimen. The mechanical properties of Young's modulus and Poisson's ratio were selected as $E = 2940$ and $v = 0.3$, respectively.

It should be noted that there were some problems in modeling the CCNSCB specimen because of high stress concentration at the two sharp corners of the notch front shown in Fig. 7a. In this figure, a is the crack length and b is the corresponding crack front width. The values of stress intensity factor at these corners became very high and inconsistent with those of the remaining points along the notch front. To overcome this problem and decrease the high stress concentration at these points, slightly rounded corners were used to model the chevron notch in ABAQUS software as shown in Fig. 7b. To find the suitable dimensions for this modified shape, several models with different dimensions were analyzed and the dimensions that were resulted in the most uniform results compared with other dimensions were chosen for the modified shape of modeling. The appropriate dimensions of the model are presented in Fig. 7b. Using this model, more uniform results could be achieved.

As mentioned before, to satisfy the plane strain conditions, the parameters related to the geometry of CCNSCB specimen should have some limitations. In order to investigate the plane strain conditions in a given sample, a path was defined in the finite element model along the crack front and then strains were calculated in three main

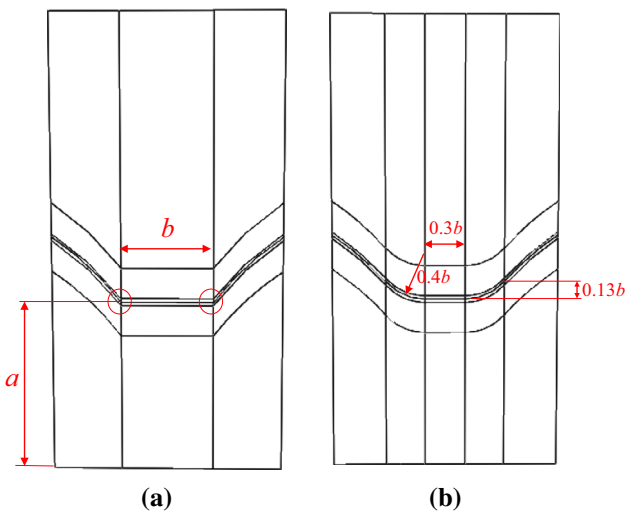

Fig. 7 Shapes of chevron notch in ABAQUS software: **a** initial modeling, **b** modified modeling

perpendicular directions along the path. The strain components in x, y, and z directions of a typical model obtained from FE analysis are plotted in Fig. 8. It can be seen that at a distance in the middle part of the crack front, strain in z direction is almost zero. Therefore, the plane strain conditions are satisfied in this specimen and the obtained fracture toughness could be considered as the plane strain fracture toughness. Also shown in Fig. 8 are the variations of ε_x along the notch front in the initial modeling (with sharp corners) in comparison with the results of modified

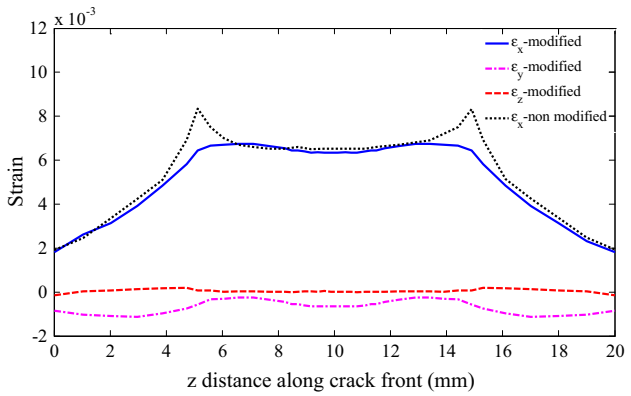

Fig. 8 Strain components in three directions along the crack front

chevron notch model. High strain concentration can be clearly seen around the two sharp corners of notch front in the initial model, as described earlier.

To compute the minimum dimensionless stress intensity factor at critical crack length, the crack length was increased gradually from its initial value. Consequently, by plotting the distribution of dimensionless stress intensity factor for different values of crack length and finding the turning point in the diagram, the critical crack length and the corresponding minimum dimensionless stress intensity factor can be obtained. For this purpose, eight different values of normalized crack length $\alpha = a/R$ were considered to analyze the CCNSCB specimen as $\alpha = 0.2$, 0.3, 0.325, 0.35, 0.375, 0.4, 0.425, 0.45, and 0.5.

Stress intensity factor could be obtained directly from FE analysis. Afterwards, using Eq. 5, dimensionless stress intensity factor could be calculated by substituting the geometry parameters and load.

The distribution of Y^* along the crack front for the sample with $\alpha = 0.3$ is plotted in Fig. 9. It can be seen that the diagram has a relatively uniform region at the middle part of the crack front and two decreasing parts at the two sides of the notch front. Since these two parts are not considered as true crack, Y^* should be determined from the middle part. In addition, there is a slight variation in the values of stress intensity factors along this part of the crack front. Therefore, the average value of Y^* at middle part was used for the CCNSCB specimen with $\alpha = 0.3$. This procedure was repeated for different values of crack length and the average of Y^* in the middle part of each case was determined. The results are summarized in Table 5.

Table 5 The values of Y^* for CCNSCB samples with different crack length ratios

	α	Y^*
Case-1	0.2	2.90
Case-2	0.3	2.31
Case-3	0.325	2.25
Case-4	0.35	2.22
Case-5	0.375	2.19
Case-6	0.3875	2.20
Case-7	0.4	2.22
Case-8	0.425	2.25
Case-9	0.45	2.34
Case-10	0.5	2.60

It is useful to remind that the two angled portions of the chevron notch are not part of the true crack, but the same special crack elements were considered along the whole notch front (including the angled portions). However, as shown in Fig. 9, after FE analysis only the middle part of the diagram was used to find the value of dimensionless stress intensity factor.

Figure 10 shows the variation of Y^* with normalized crack length α. The minimum value of Y^* presents the minimum dimensionless stress intensity factor $Y^*_{\min}$, when the crack length reaches its critical value (normalized critical crack length-α_m).

It can be observed from this figure that Y^* in CCNSCB specimen first decreases and then, after reaching a critical value of crack length, increases as the crack length becomes larger. In fact, due to the high stress concentration

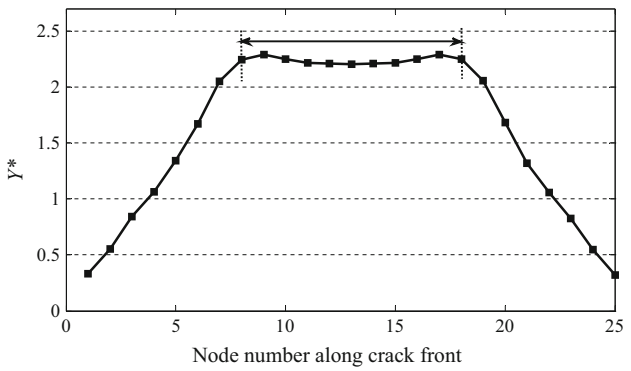

Fig. 9 Distribution of Y^* along the crack front for CCNSCB specimen with $\alpha = 0.3$

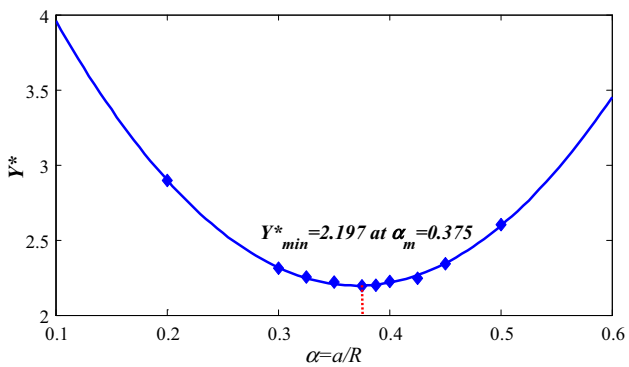

Fig. 10 Variation of Y^* with crack length ratio for the CCNSCB specimen

at the tip of chevron notch, the crack initially grows in a sub-critical manner. Thereafter, unstable crack growth occurs rapidly and final failure takes places in the specimen.

A second order polynomial can be fitted to Y^* as shown by Eq. 6.

$$Y^* = 5.50 - 17.81\alpha + 24\alpha^2 \tag{6}$$

To identify the critical crack length, $Y^*_{\min}$ was determined by setting the derivative of this equation to zero. One of the roots was 0.375 as normalized critical crack length. Thereafter, $Y^*_{\min}$ can be obtained from Eq. 6. In this case, we obtained $Y^*_{\min} = 2.197$ at $\alpha_m = 0.375$.

2.2.3 *Determination of Y* in CCNSCB using slice synthesis method*

Slice synthesis method (SSM), proposed first by Bluhm (1975), is a semi-analytical method in which the thickness of specimen is divided into a number of slices. Each slice is considered as a cracked straight through specimen that is simpler than the complex configuration of chevron notched specimens to be analyzed. Based on this method, analysis is carried out for each slice and then by combining the equations, an analytical correlation could be obtained for the whole specimen based upon the equilibrium principle. Using this method, appropriate analytical relations for complex configurations can be extracted. At first, the output of this method was the compliance, which could eventually lead to measuring the stress intensity factor by means of the compliance function relationship with the stress intensity factor. However, in a geometrically complicated specimen like the CCNBD or CCNSCB, it is difficult to obtain the compliance function (related to the section of sample without crack). For instance, a constant term related to the part of the specimen without crack was neglected for computing the stress intensity factor of CCNBD specimen (Bluhm 1975). Later, a new slice synthesis method was proposed to solve the problem and to obtain the stress intensity factor directly (Wang et al. 2004).

Wang et al. (2004) determined the stress intensity factor of CCNBD specimen from this new procedure of slice synthesis method with small corrections using an empirical factor. This procedure has a better precision for a wider range of geometric parameters. In the following, the same procedure is used for the CCNSCB specimen.

At the beginning, CCNSCB specimen, as shown in Fig. 11, is divided into several slices along its thickness. Each slice could be considered as a CSTSCB specimen with thickness Δt, while there is no need to divide the central part of the specimen with thickness b; because it is itself considered as a SCB specimen with a straight crack front of width b. Now, using Eq. 1, the applied force can be calculated in each slice.

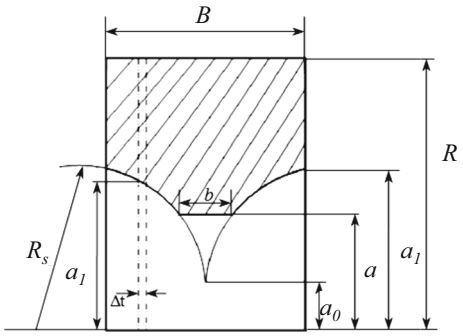

Fig. 11 Slice synthesis method for CCNSCB specimen

It should be noted that Eq. 1 has been suggested for a crack, while, as shown in Fig. 11, only the central part of the specimen that is formed due to crack growth is a real crack. Therefore, the stress intensity factor of central part is considered as K_I. However, the two lateral chevron parts are not real cracks and thereby, the stress intensity factor for each of these slices has a lower value than K_I. Therefore, a reduction factor for the slices other than the central part should be employed, i.e.,

$$K'_I = \begin{cases} K_I & \text{central slice} \\ K_I/\beta & \text{other slices} \end{cases} \tag{7}$$

As an empirical factor, β is always greater than one.

Therefore, using Eqs. 1 and 7 and summing up the loads applied on each slice, the total load can be obtained as:

$$P = \frac{K_I.2Rb}{\sqrt{\pi a}\,Y_I(\alpha)} + \sum_{i=1}^{N} \frac{K_I.(2R.\Delta t)}{\beta\sqrt{\pi a}\,Y_I(\alpha_i)}, \tag{8}$$

where Δt and N are the thickness of each slice and the number of slices, respectively. Y_I is the dimensionless stress intensity factor of CSTSCB and $\alpha_i = a_i/R$, where a_i is the crack length of ith slice.

Parameters Δt, α_i and b are related to the normalized critical crack length (α_m). The first term in Eq. 8 is related to the central part of specimen with the normalized crack length α and the crack width b, and the second term is associated with the lateral slices with different normalized crack lengths α_i.

The thickness of the central part of specimen can be calculated by means of the following geometric relationships

$$b = 2R\left(\sqrt{\alpha_s^2 - \alpha_0^2} - \sqrt{\alpha_s^2 - \alpha^2}\right) \tag{9}$$

The thickness, Δt and the normalized crack length α_i of each slice could also be calculated as follows:

$$\begin{cases} \Delta t = \dfrac{B-b}{N}, \\ \alpha_i = \sqrt{\alpha_s^2 - \left(\sqrt{\alpha_s^2 - \alpha_0^2} - \dfrac{b}{2R} - \dfrac{i.\Delta t}{R}\right)^2}, \end{cases} \tag{10}$$

where i is the slice number from the center of the specimen apart of the central part having the flat notch.

By rewriting Eq. 5, the following relation for the dimensionless stress intensity factor of CCNSCB specimen can be obtained

$$Y_I = \frac{K_I B\sqrt{R}}{P} \tag{11}$$

Substituting Eq. 8 into Eq. 11, the dimensionless stress intensity factor of CCNSCB specimen could be calculated as:

$$Y^* = \left[\frac{2b/B}{\sqrt{\pi\alpha}Y_I(\alpha)} + \sum_{i=1}^{N/2}\frac{4.\Delta t/B}{\beta\sqrt{\pi\alpha_i}.Y_I(\alpha_i)}\right]^{-1} \tag{12}$$

The empirical factor of β, of a chevron notched specimen was proposed as below for CCNBD (Wang 1998)

$$\beta = 1 + \gamma\frac{\alpha_1 - \alpha}{\alpha_B} \tag{13}$$

One of the important steps of SSM procedure is the appropriate determination of the reduction factor β, which depends on the crack geometry. For instance, by comparing with the results of three-dimensional finite element analysis, Wang et al. (2004) predicted the value of γ in Eq. 13 as 0.9 for the CCNBD specimen.

This parameter expresses the difference between the stress intensity factor of the central part and those of the lateral sections. Therefore, it depends directly on the notch geometry. As reported by Mahdavi et al. (2015), for CCNSCB with V-shaped notch (linear chevron shape), Eq. 13 can be used by taking $\gamma = 0.85$. However, for CCNSCB with curved chevron notch (Fig. 1), it was found from FE results that the value of $Y^*_{\min}$ obtained from Eq. 13 is not acceptable. Therefore, a new form of Eq. 13 is proposed to estimate the coefficient β as

$$\beta = 1 + \gamma\left(\frac{\alpha_1 - \alpha}{\alpha_B}\right)^n \tag{14}$$

Employing three-dimensional finite element analysis of the CCNSCB specimen in mode-I loading and using SSM for a similar SCB specimen and then comparing the results, the coefficient γ and the power n in the CCNSCB specimen were estimated as 0.9 and 0.5, respectively. Since the minimum value of the stress intensity factor is used to calculate the mode-I fracture toughness, the minimum value of Eq. 12 is determined by putting its derivative with respect to the normalized crack length α equal to zero.

Having the dimensionless geometric parameters (α_S, α_0, α_1, and α_B) and substituting them into Eq. 12 to utilize SSM for the CCNSCB specimen, the dimensionless stress intensity factor relation can be obtained. It should be noted that $Y_I(\alpha)$ in Eq. 12 is the dimensionless stress intensity factor in CSTSCB specimen which is determined from Eq. 3. For the specimen considered here ($\alpha_0 = 0.175$, $\alpha_1 = 0.52$, $\alpha_S = 0.625$, $\alpha_B = 0.5$, and $S/R = 0.5$), by calculating the minimum value of Eq. 12 using a numerical analysis software, the minimum stress intensity factor was obtained as $Y^*_{\min} = 2.120$ at $\alpha_m = 0.384$.

In Table 6, the values of α_m and $Y^*_{\min}$ obtained from two different methods are compared. As can be seen from this table, both the SSM and FEM methods can provide very closely related values for the critical crack length, with a small discrepancy of 3.50 %. Thus, one may conclude that both methods are able to evaluate the stable crack growth in cracked chevron notch semi-circular bend specimens.

Figure 12 presents the variations of dimensionless stress intensity factors with the normalized crack length α obtained from SSM method (Eq. 12) and finite element analysis. The minimum dimensionless stress intensity factors determined from these two methods are also compared in this figure.

It can be observed from Fig. 12 that the stress intensity factor in CCNSCB specimen first decreases and then increases as the crack grows. This process can be explained as follows: the crack growth occurs sub-critically due to the

Table 6 The values of α_m and $Y^*_{\min}$ for CCNSCB specimens obtained from the SSM and FE analysis

	$Y^*_{\min}$	α_m
SSM	2.120	0.384
FEM	2.197	0.375
Discrepancy	3.50 %	2.4 %

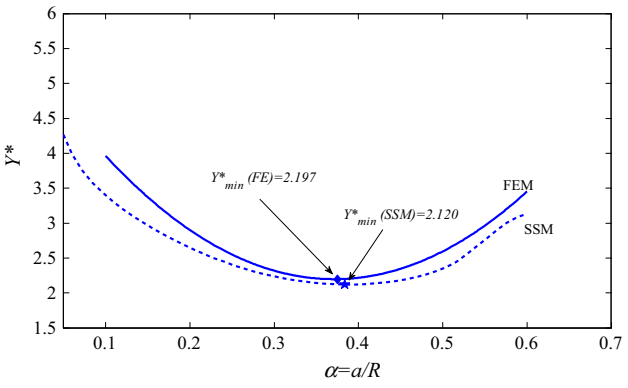

Fig. 12 The variations of mode-I dimensionless stress intensity factor of CCNSCB determined using both slice synthesis method and FEM

Table 7 The calculated values of fracture toughness for CCNSCB specimens of Vietnam white marble

Test no.	P_{max} (kN)	$K_{Ic}(\mathrm{MPa}\sqrt{m})$
1	1.914	1.051
2	1.82	1.000
3	1.8	0.989
4	1.871	1.028
5	1.876	1.030
6	1.981	1.088
Average		1.031

high stress concentration at the tip of chevron notch; then, it extends stably inside the plane of chevron notch until the crack length reaches its critical value ($a \leq a_m$). Indeed, V or chevron shape of notch generates stable crack growth from the initial crack length (a_0) to its critical length (a_m). After that, the force decreases and unstable crack growth occurs rapidly and the final failure takes place in the specimen. The chevron notches provide sharper critical cracks from the tip of notch, which are suitable for stabilizing the crack growth as well as developing stress intensity factors of higher precisions and lower scatter. Thereby, this specimen can be a good choice for predicting the fracture toughness of rock masses and investigating the process of crack growth in brittle and quasi-brittle materials.

Using the fracture loads given in Table 4 and the minimum dimensionless stress intensity factor $Y^*_{min} = 2.197$, fracture toughness was determined from Eq. 5 for each experiment performed on CCNSCB specimens of Vietnam white marble as described earlier. Table 7 shows the calculated values of fracture toughness for each specimen. Also given in this Table is the average fracture toughness of 1.031 $MPa\sqrt{m}$ which is in good agreement with the values reported by Hsieh and Wang (2004) between 1.03 and 1.35 $MPa\sqrt{m}$ for a similar material but tested at different loading rates.

3 Conclusions

One of the experimental specimens for obtaining rock fracture toughness is semi-circular bend specimen which has recently received much attention by researchers. In the first part of this paper, useful relations were suggested for evaluating the dimensionless stress intensity factor of the CSTSCB specimen through finite element analysis of a large number of SCB specimens with different values of crack lengths and half distances between the supports. Since the procedure employed for calculating the stress intensity factors is based on the J-integral method, the presented equations could precisely predict the mode-I dimensionless stress intensity factor and, the mode-I fracture toughness.

Moreover, analytical and numerical methods were used to analyze the dimensionless stress intensity factor of CCNSCB specimen. Some experiments were conducted to obtain the experimental peak load that must be employed in finite element analysis of CCNSCB specimen. Afterwards, using the SSM method which have been previously used for determining the stress intensity factors of BD and SR specimens, the dimensionless stress intensity factor of the CCNSCB specimen was obtained. Furthermore, the validity and accuracy of this analytical method was investigated through finite element results. The chevron shaped notch in the cracked chevron notched specimens generates a sharp crack, due to the limited stage of stable crack growth. It was shown that the SSM method could provide very good estimations for the dimensionless stress intensity factor in the CCNSCB specimen.

References

Ayatollahi MR, Aliha MRM (2006) On determination of mode II fracture toughness using semi-circular bend specimen. Int J Solids Struct 43:5217–5227

Ayatollahi MR, Aliha MRM, Hassani MM (2006) Mixed mode brittle fracture in PMMA—an experimental study using SCB specimens. Mater Sci Eng A 417:348–356

Ayatollahi MR, Aliha MRM, Saghafi H (2011) An improved semi-circular bend specimen for investigating mixed mode brittle fracture. Eng Fracture Mech 78:110–123

Bluhm JI (1975) Slice synthesis of a three dimensional work of fracture specimen. Eng Fracture Mech 7:593–604

Chong KP, Kuruppu MD, Kuszmual JS (1987) Fracture toughness determination of layered materials. Eng Fracture Mech 28(1):43–54

Fowell RJ (1995) Suggested method for determining mode I fracture toughness using cracked chevron notched Brazilian disc (CCNBD) specimens. Int J Rock Mech Min Sci Geomech Abstr 32:57–64

Hsieh CT, Wang CL (2004) The measurement of the crack propagation in rock slabs. In: Proceedings of the ISRM international symposium 3rd ARMS, Rotterdam, Netherlands

Kanninen MF, Popelar CH (1985) Advanced Fracture Mechanics. Oxford Engineering Science Series (15). Oxford University Press, New York

Kuruppu MD (1997) Fracture toughness measurement using chevron notched semi-circular bend specimen. Int J Fract 86(4):33–38

Kuruppu MD (1998) Stress intensity factors of chevron-notched semi-circular specimens. In: Basu et al (eds) Proceeding of 3rd APCOM, the austinst of min and met, pp 111–112

Kuruppu MD (2000) Fracture toughness testing of geomaterials using semi-circular specimen. In: Proceeding of geo engng, Technomic Publishing Lancaster vol. 2

Kuruppu MD, Obara Y, Ayatollahi MR, Chong KP, Funatsu T (2014) ISRM-suggested method for determining the mode I static fracture toughness using semi-circular bend specimen. Rock Mech Rock Eng 47(1):267–274

Kuruppua MD, Chong KP (2012) Fracture toughness testing of brittle materials using semi-circular bend (SCB) specimen. Eng Fract Mech 91:133–150

Lim IL, Johnston IW, Choi SK (1993) Stress intensity factors for semi-circular specimens under three-point bending. Eng Fract Mech 44:363–382

Lim IL, Johnston IW, Choi SK, Boland JN (1994) Fracture testing of a soft rock with semi-circular specimens under three-point loading, Part 1 – Mode I. Int J Rock Mech Min Sci 31:185–197

Mahdavi E, Obara Y, Ayatollahi MR (2015) Analysis of stress intensity factor of semi-circular bend specimen with chevron notch by finite element method. In: Proceeding of MMIJ, Chiba, Japan

Matsuki K, Hasibuan SS, Takahashi H (1991) Specimen size requirements for determining the inherent fracture toughness of rocks according to ISRM suggested methods. J Appl Mech 18:413–427

Ouchterlony F (1988) ISRM Suggested methods for determining fracture toughness of rocks. Int J Rock Mech Min Sci Geomech Abstr 25:71–96

Tutluoglu L, Keles C (2011) Mode I fracture toughness determination with straight notched disk bending method. Int J Rock Mech Min Sci 48:1248–1261

Wang QZ (1998) Stress intensity factors of ISRM suggested CCNBD specimen used for mode-I fracture toughness determination. Int J Rock Mech Min Sci 35:977–982

Wang QZ, Jia XM, Wu LZ (2004) Wide-range stress intensity factors for the ISRM suggested method using CCNBD specimens for rock fracture toughness tests. Int J Rock Mech Min Sci 41:709–716